VALIDATION AND CROSS-VERIFICATION OF THREE MECHANISTIC CODES FOR ANNULAR TWO-PHASE FLOW SIMULATION AND DRYOUT PREDICTION

L. Sanmiguel Gimeno, S. P. Walker, G. F. Hewitt
Imperial College London
SW7 2AZ, London, UK
ls2011@imperial.ac.uk; s.p.walker@imperial.ac.uk; g.hewitt@imperial.ac.uk

J.-M. Le Corre
Westinghouse Electric Sweden AB
72163, Västerås, Sweden
lecorrjm@westinghouse.com

A. Dasgupta
Bhabha Atomic Research Centre
Mumbai, 400085, India
arnie@barc.gov.in

M. Ahmad
Pakistan Institute of Engineering & Applied Sciences,
Islamabad, Pakistan
fac134@pieas.edu.pk

ABSTRACT

The ability to predict the boiling transition, or dry-out, in annular two-phase flow is essential to Light Water Reactor (LWR) safety analysis. Common approaches include the use of empirical correlations or look-up tables which, although reliable, cannot be readily applied to complex cases outside the experimental range used for their development. Phenomenological models can widen the range of conditions in which dry-out can be predicted as they provide a better insight into the governing phenomena. These models however also employ empirical correlations to close the system of conservation equations and therefore require validation against experimental data.

In this paper, three independently-developed codes for the phenomenological modelling of dry-out, GRAMP, MEFISTO-T and SCADOP, are compared against one another and validated against two experimental dry-out datasets. These data, on dry-out in tubes, were generated by BARC, in India, and Harwell, in the UK. The three codes are used to predict the location of: the onset of annular flow, the film flow rate along the annular flow length, the dry-out power and the location of dry-out under broadly BWR operating conditions. A high level of consistency between the three codes is demonstrated, and good agreement is observed against the experimental data. Some areas of uncertainty are also discussed in this paper, with the focus on the applicability of the entrainment-deposition correlations and the importance of the liquid entrained fraction at the onset of annular flow.

KEYWORDS
Annular two-phase flow, dry-out, three-field model, phenomenological model

1. INTRODUCTION

Critical Heat Flux (CHF), often referred to as "dry-out" or "burnout" in the literature, relates to the event which causes a sudden drop in the efficiency of heat transfer from a surface, leading to a drastic rise in the temperature of that surface. Such a drop in efficiency is caused by a persistent change from liquid to vapour being in contact with the heated surface. Reliable knowledge of the margin to CHF is essential in Light Water Reactor (LWR) design and operation. The present work focuses on "film dry-out" in annular flow, one of the main forms of CHF, and the most relevant to Boiling Water Reactor (BWR) operation. Two-phase flows are complex in nature and exist in many different regimes depending on flow rates, pressure and flow passage diameter. Methods to predict dry-out in annular flow include the use of empirical correlations [1], look-up tables [2] and phenomenological modelling [3], all of which are empirical to some extent.

In this paper, three independently-developed codes for the mechanistic prediction of CHF in annular flow are cross-verified and validated against two sets of experimental data. Several phenomenological dry-out prediction codes of varying complexity exist, but to the authors' knowledge only one other benchmark between mechanistic prediction codes has been carried out and documented before [4].

The phenomenological model for steady-state annular flow is a simple one-dimensional model with ordinary differential equations to solve for each field. The solution for dry-out depends on the initial conditions, (i.e. at the onset of annular flow) and the knowledge of the flow rates of each field (film, droplets and vapour). Even though the governing equations are relatively simple, modifications and adjustments are made to each code by the developer to satisfy each specific application. Therefore, code comparison against experimental data checks the validity of the approach taken in each code and cross-verification between the codes analyses the performance of each approach when compared to other codes. In addition, a sensitivity analysis has been carried out on the value of the liquid entrained fraction at the onset of annular flow, one of the most important yet most uncertain boundary conditions in annular flow modelling. This analysis reveals that the current entrainment deposition correlations still have potential for improvement.

In section 2, phenomenological modelling is introduced, discussed, and the three considered codes are presented. Section 3 describes the experimental data used for the verification, and the simulation results are discussed in section 4. An initial liquid entrained fraction (IEF) analysis follows in section 5 and conclusions are presented in section 6.

2. PHENOMENOLOGICAL MODELLING

The phenomenological modelling approach complements empirical correlations and the look-up tables as a method to predict dry-out. It seeks to employ independent empirical correlations to describe the two individual phenomena contributing to dry-out, namely droplet entrainment from the film, and droplet deposition onto the film. Such constitutive relations provide closure to the system of conservation equations for the flow rate of liquid in the annular liquid film and the flow rate of droplets entrained in the vapour core.

The main motivation behind phenomenological modelling follows from cases that cannot be predicted by the sole use of empirical correlations due to a limited experimental database used in their development. These include non-uniform axial variation of power or transient conditions [5]. The applicability and reliability of the phenomenological model is limited by how general the constitutive relations, used to describe the phenomena, are. For full reactor modelling, the computational time can also be a limiting factor [5]. Three phenomenological codes are described below.

2.1. MEFISTO-T

MEFISTO-T (Mechanistic Film Sub-Channel Tool - Transient) is a phenomenological modelling tool developed at Westinghouse Electric Sweden to determine the film flow distributions on every rod in a

BWR fuel bundle, under steady-state or transient conditions. The code is coupled onto the results of the driver two-field sub-channel code (VIPRE-W) that calculates the mass and enthalpy distributions in each sub-channel. The aim behind this approach is to increase the flexibility and reduce the computational time required for full BWR fuel modelling. A more thorough description of MEFISTO-T and the associated validation can be found in [5] and [6].

2.2. SCADOP

SCADOP (Subchannel Analysis and Dryout Prediction) was developed at BARC, India to predict dry-out in fuel rod bundles mechanistically. SCADOP was developed by combining a tubular film flow module, DROPIT [7], with a driver sub-channel code [8]. The phenomenological model solves for mass conservation in the film, droplet and vapour fields, in order to arrive at the dry-out condition, and is only applicable to annular flow. The full validation can be found in [9].

2.3. GRAMP

GRAMP (General Runge-Kutta Annular Modelling Program) was developed over several PhD theses at Imperial College London. Its initial application was to model hydrocarbon flows for the oil industry, however the most recent work on GRAMP has been concerned with thermal hydraulics for nuclear reactor application. GRAMP models the pre-annular flow regimes to predict flow regime transitions. Unlike MEFISTO-T or SCADOP which solve for the mass flow rates of each separate field, GRAMP solves equations for the liquid entrained fraction and thermodynamic quality. A more thorough description and validation can be found in [3].

3. EXPERIMENTAL DATA AND FLOW REGIME MAP

The two sets of experimental data, used for the validation of the three codes, were obtained in high pressure steam-water facilities. In both sets of experiments, water at high pressure was pumped up a circular heated section where it was allowed to boil. The heat was provided by a uniform axial current on the walls of the test sections. The applied power was increased in small steps until dry-out was detected. For the BARC measurements, thermocouples were placed on the walls of the section to detect the characteristic temperature spike of CHF [10]. In the case of the Harwell experiments, differential measurements of the section's electrical resistance were used to detect CHF [11]. More thorough descriptions of the test rigs and experimental conditions can be found in the aforementioned references. The range of the experimental measurements is summarised in Table I.

Table I – Range of conditions used in the BARC and Harwell experiments

	BARC [12]	**Harwell [13]**
Pressure (bar)	29-71	67-71
Mass flux (kg m^{-2} s^{-1})	820-1700	620-2000
Diameter (mm)	8.8	12.6
Length (m)	3.5	1.82-5.56
Inlet Sub-cooling (K)	10-45	5-110
Heat flux (kW m^{-2})	832-1220	580-2000
Exit quality (-)	0.57-0.93	0.39-0.95
Boiling length (m)	2.9-3.4	1.2-5

The most common way to identify flow regimes is by visual examination. Hewitt and Roberts [13] compiled their experimental observations into a flow regime map that defines regime transitions in terms of the superficial liquid and vapour momentum fluxes; see Figure 1. The process of defining regime transitions is highly subjective, but nevertheless, this map provides a good insight into the

proximity to a regime transition. On Figure 1 are shown also all the data points from Table I at dry-out. As expected, the data lies in the annular flow region, relatively far from both the churn flow region and the wispy-annular flow region.

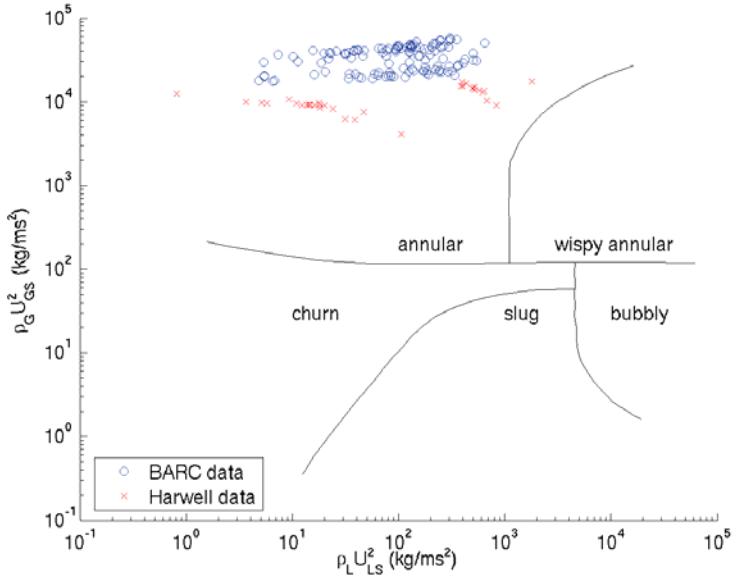

Figure 1. The experimental data to be analysed, from BARC (blue circles), and Harwell (red crosses) plotted on the flow regime map of Hewitt and Roberts [13]

4. SIMULATION RESULTS

4.1. Simulation Models

In order to solve the balance equations, expressions to describe the entrainment, deposition and evaporation phenomena are required. A very brief description of the entrainment, deposition and evaporation rates are provided in this section as this paper focuses on the performance of the codes rather than on the underlying correlations.

4.1.1. Entrainment and Deposition Correlations

There are various entrainment and deposition correlations available in the literature (e.g. [14], [15] ,[16]), but for the present work, the entrainment and deposition correlations selected for integration into the three phenomenological models are those developed by Govan and Hewitt [17]. In this correlation, the deposition rate of droplets on the film is treated as being controlled by diffusion processes and is given by equation (1)

$$D = k_D C \tag{1}$$

where C is the concentration of droplets in the core given by equation (2).

$$C = \frac{G_{LE}}{\frac{G_G}{\rho_G} + \frac{G_{LE}}{\rho_L}} \tag{2}$$

The droplet deposition coefficient k_D is given by equation (3).

$$k_D = \begin{cases} 0.18\left(\dfrac{\sigma}{\rho_G d}\right)^{0.5} & ;\ \text{if } \dfrac{C}{\rho_G} \le 0.3 \\ 0.083\left(\dfrac{\sigma}{\rho_G d}\right)^{0.5}\left(\dfrac{\rho_G}{C}\right)^{0.65} & ;\ \text{if } \dfrac{C}{\rho_G} > 0.3 \end{cases} \tag{3}$$

The entrainment rate of droplets from the film into the core is given by equation (4)

$$E = \begin{cases} 0 & ;\ \text{if } G_{LF} \le G_{LFC} \\ 5.75\times10^{-5}\times G_G\left(\dfrac{d\rho_L}{\sigma\rho_G^2}\left(G_{LF}-G_{LFC}\right)^2\right)^{0.316} & ;\ \text{if } G_{LF} > G_{LFC} \end{cases} \tag{4}$$

where G_{LFC} represents the critical film flow rate below which no entrainment occurs.

$$G_{LFC} = \frac{\mu_L}{d}\exp\left(5.8504 + 0.4249\left(\frac{\mu_G}{\mu_L}\right)\left(\frac{\rho_L}{\rho_G}\right)^{0.5}\right) \tag{5}$$

4.1.2. Evaporation rate

The evaporation rate in the three codes follows from a steady state assumption in which the film is taken to be at saturation conditions at its surface, and all the heat from the walls acts to evaporate the liquid film at that axial location.

4.1.3. Onset of Annular Flow

In order to start the integration for the annular flow regime, conditions at the onset of annular flow must be identified. For the present work, the three codes were set to use the empirical correlation by Wallis [18] which characterises the onset of annular flow in terms of the superficial vapour flux and is given by equation (6)

$$u_{GS}^{*} = u_{GS}\sqrt{\frac{\rho_G}{gd\left(\rho_L-\rho_G\right)}} = 1 \tag{6}$$

GRAMP solves for the superficial velocity up the channel while MEFISTO-T and SCADOP both solve for the thermodynamic quality.

4.1.4. Initial entrained fraction

The initial entrained fraction (IEF) refers to the fraction of the liquid that is in the droplet field at the onset of annular flow and can, in principle, take any value between zero and unity. As will be discussed in more detail in section 5, the value of the IEF is very difficult to measure experimentally, as is evident from the scarce research in the field. For the present cross-verification and validation, a value for the IEF of 0.7 has been first assumed following the recommendation from the previous

GRAMP validation [3]. However, the basis of the recommendation is necessarily a little tenuous, and other methods to predict the IEF are discussed in section 5.

4.1.5. Dry-out condition

For the three codes, the condition for dry-out has been defined as the point at which the film flow rate drops to zero. Given their varying underlying formulations, each code implements this condition in a different way. For MEFISTO-T, dry-out is taken as being when the absolute value of the film flow rate is less than 0.00005 kg/s. GRAMP takes dry-out to be when the film flow rate is less than 0.1% of the total mass flux, and SCADOP when the film flux is less than or equal to 0.00001 kg/m^{2}s. For practical purposes, these criteria amount to the same thing.

4.1.6. Prediction procedure

There are multiple ways in which to use the codes to analyse dry-out data. The ultimate purpose of these codes is to determine the critical power and the location of dry-out as accurately as possible for any given axial power distribution. In the case of uniform axial power distribution, dry-out always occurs at the exit of the heated sections and the corresponding critical power is known from the experimental data used in this validation. In the simulations, the power was incremented until the dry-out condition was detected at the last node. The results were recorded and compared to the experimental power (or average heat flux).

4.1.7. Main code characteristics

A brief summary of the main characteristics of each code can be found in Table II.

Table II – Summary of the main parameters and models used by each code

	MEFISTO-T	GRAMP	SCADOP
Applicable Flow regimes	Annular Flow only	Bubbly, Slug, Churn, Annular	Annular Flow only
***Entrainment - Deposition correlations**	Govan-Hewitt [17]	Govan-Hewitt [17]	Govan-Hewitt [17]
***Onset of Annular flow condition**	Wallis [18]	Wallis [18]	Wallis [18]
***Initial Entrained Fraction**	0.7	0.7	0.7
Dry-Out condition	$m_{lf} \leq 0.00005\ kg/s$	$\frac{G_{lf}}{G} \leq 0.001$	$G_{lf} \leq 0.00001 \frac{kg}{m^2 s}$
Pressure Drop	Calculated by driver sub-channel code	Integrated by GRAMP	Calculated by driver sub-channel code
Enthalpy Distribution	Calculated by driver sub-channel code	Integrated by GRAMP	Calculated by driver sub-channel code
Physical Properties	Calculated by driver sub-channel code	Integrated by GRAMP from the pressure and temperature at each node	Constant properties evaluated from property table at a single system pressure
Numerical Scheme	First-order up-wind scheme	Fourth Order Runge-Kutta	First order space-marching

In this table, the parameters marked with an asterisk indicate models that were purposely chosen to be identical. These parameters are application-specific and can cause the codes to give different predictions. By applying the same models, any possible code difference due to other reasons such as numerical scheme, model implementation or simplifications can be identified.

4.2. CHF Predictions of the BARC and Harwell Data

4.2.1. Validation

The purpose of the validation is to provide evidence that the phenomenological modelling codes can be used to predict dry-out cases. Of necessity to predict measurement well, the models must have been properly implemented, but more importantly, validation indicates whether the theoretical approach and empirical correlations used in the development of the model provide a good description of the governing phenomena. Figure 2 shows the dry-out power predictions of the three codes for the BARC data against the experimental power measurements, and Figure 3 shows the predictions for the Harwell data against the experimental measurements in the same format. Table III shows the mean error, root mean square error and standard deviation for each code for each data set separately and for the full data set.

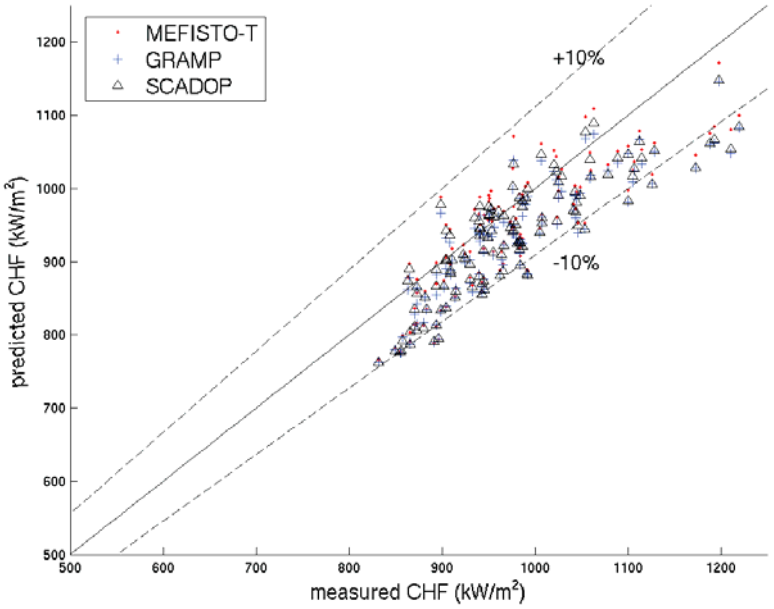

Figure 2. Data from BARC predicted by MEFISTO-T, GRAMP and SCADOP.

Figure 2 and Figure 3 show that the three codes predict values of CHF following a similar trend: a slight under-prediction at lower values of CHF which turns into a slight over-prediction at higher values of CHF. The three codes solve broadly the same constitutive relations, and use the same boundary conditions and so this similarity in prediction is not unexpected. From Table III it can be seen that the absolute value of the mean error for the three codes is below 3% and the magnitude of the largest RMS error is below 8%. The three codes can predict all the data points within 11%. When both datasets are combined, the lowest mean error is of -1.86% from MEFISTO-T, the lowest RMS error is of 5.89% from SCADOP and the lowest standard deviation is of 3.61% from GRAMP.

Table III. Errors in the MEFISTO-T, GRAMP and SCADOP predictions

	MEFISTO -T			GRAMP			SCADOP		
In %	**BARC**	**Harwell**	**Total**	**BARC**	**Harwell**	**Total**	**BARC**	**Harwell**	**Total**
Mean error	-3.19	2.69	-1.86	-4.63	2.91	-2.94	-4.09	0.75	-3.06
RMS error	5.73	7.61	6.15	6.28	6.86	6.41	6.02	5.43	5.89
Standard deviation	4.76	1.14	3.95	4.25	1.41	3.61	4.42	1.19	3.73

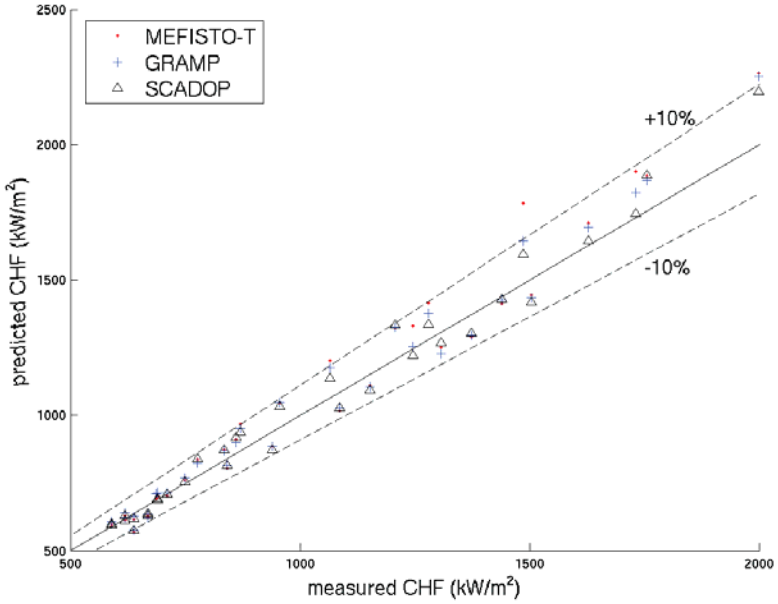

Figure 3. Data from Harwell predicted by MEFISTO-T, GRAMP and SCADOP.

4.2.2. Cross-verification

The cross-verification between the codes provides a good way of comparing the effectiveness of the modelling approach taken for each code. A cross-verification is only meaningful following a validation. From Figure 2 it can be seen that MEFISTO-T tends to predict slightly higher dry-out powers compared to GRAMP and SCADOP. This effect becomes more evident at the higher values of CHF for the BARC data.

Table IV shows the errors between the codes. Despite the difference in predictions seen in Figure 2 and Figure 3, the mean error is always below 1.2%, the RMS error below 2.1% and the standard deviation below 1.4%, all of which are well below the 11% band that covers all the data points. In broad terms, the codes are much closer to each other than, taken together, they are to the measured behaviour.

Table IV. Errors of each code compared to one another

	Mean error				RMS error				Standard deviation		
In %	**MEF**	**GRA**	**SCA**		**MEF**	**GRA**	**SCA**		**MEF**	**GRA**	**SCA**
MEFISTO-T		-1.094	-1.006			1.908	1.592			1.324	1.167
GRAMP	1.138		0.321		2.016		1.428		1.396		1.174
SCADOP	1.041	-0.085			1.666	1.408			1.232	1.151	

Figure 4 shows the quality, liquid flow rate and steam flow rate computed by each code for a particular BARC case. The computed quality and flow rates are the same for MEFISTO-T and SCADOP but slightly different for GRAMP. The main difference is observed from the inlet and is therefore linked to the conversion between inlet temperature (boundary condition) and inlet enthalpy

(and quality). This could be due to the use different steam tables by the codes (MEFISTO-T and SCADOP use different steam tables and GRAMP uses property functions.) A difference in thermodynamic quality distribution immediately leads to a change in the onset of annular flow and hence a change in the film flow distribution.

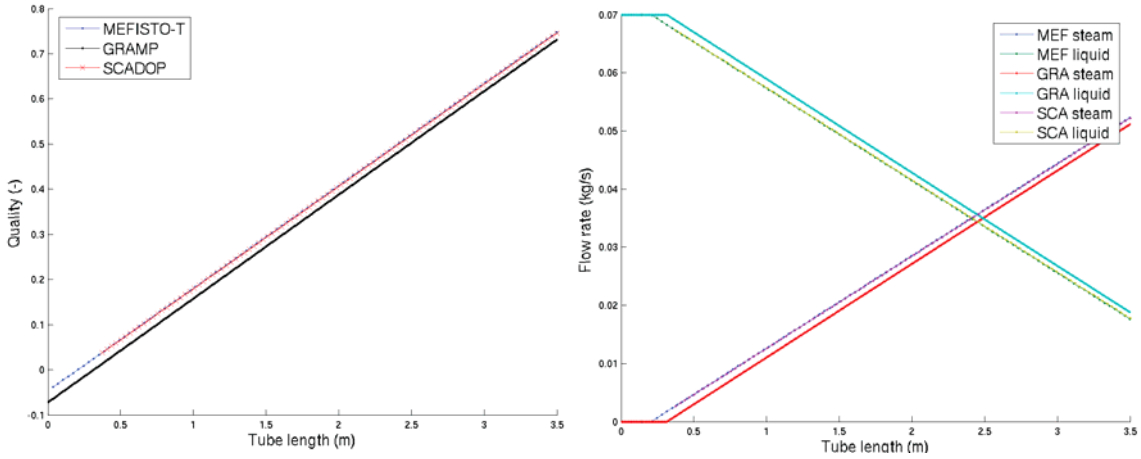

Figure 4. Quality (left) and liquid and steam densities (right) computed by each code at each elevation.

Figure 5 shows the film and droplet flow rates computed by each code for the same BARC case as before. It can be seen that the film and droplet flow rates follow the same trend but that there is a shift in the onset of annular flow prediction between the codes, as mentioned earlier. This, in part, explains why the codes do not provide exactly the same dry-out power predictions. A separate calculation was performed using the same inlet enthalpy in the MEFISTO-T and GRAMP codes for the selected case. The results show that the codes predicted the same film flow and dry-out power. In light of this comparison, it is concluded that, when using the same set of closure relations and boundary conditions, these codes are essentially equivalent.

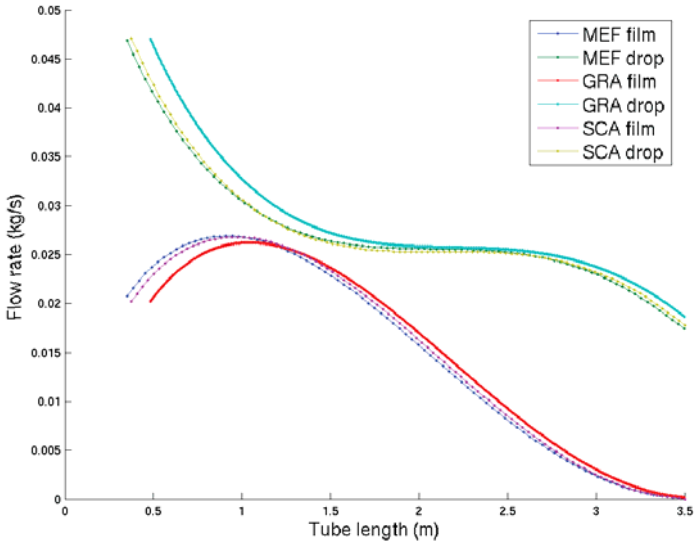

Figure 5. Film and droplet flow rates computed by each code at each elevation, from onset of annular flow to outlet

5. IEF SENSITIVITY ANALYSIS

5.1. Importance of the IEF

As mentioned in section 4.1.4, the value of the IEF is one of the most uncertain boundary conditions in the phenomenological modelling of annular flow. The importance of a correct estimate of the IEF at the onset of annular flow has been already highlighted in the literature for short annular flow lengths and for high mass fluxes [19], [3].

Figure 6 shows how the predicted CHF by MEFISTO-T varies with the IEF for different mass fluxes and different tube lengths. For constant tube length, the predictions are more sensitive to the IEF for the higher mass flux case, and similarly, for constant mass flux, the predictions are more sensitive for the shorter tube lengths. As can be seen from the four cases, a single value of the IEF cannot represent all the data. In two instances, no dryout can be predicted within the physical range of IEF. Work on improving the prediction of the IEF has been carried out the past [20], [21] and it has also been suggested that there might be advantages to starting the integration from the onset of churn flow to provide a more mechanistic calculation of the IEF [22], [23]. This is an area of active research.

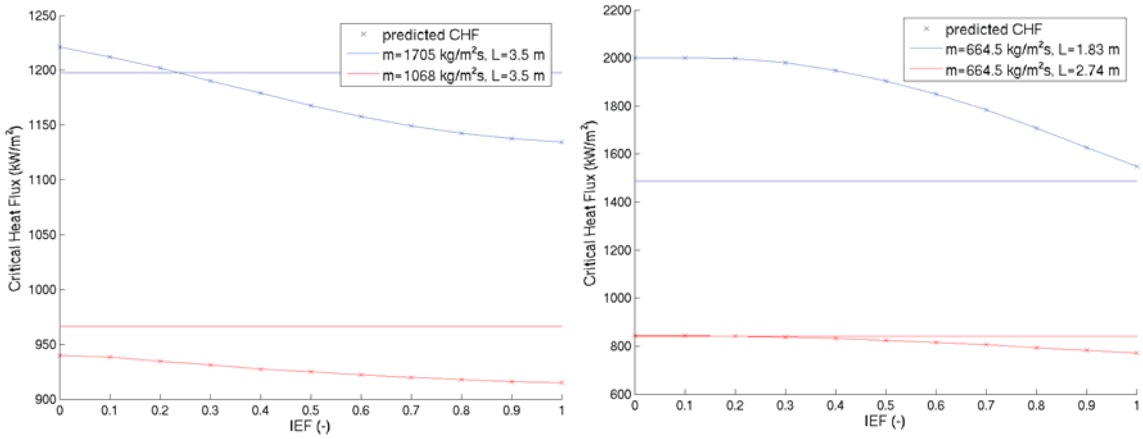

Figure 6. Variation of CHF prediction with IEF for different mass flux and different elevation

5.2. Iteration on the IEF

In this validation, a fixed value for the IEF was chosen based on previous recommendation, but it is unlikely that a single value of the IEF will be correct for the onset of annular flow conditions for each possible experimental case, and even less for reactor operating conditions. For this reason, the IEF was iterated in an attempt to identify the value of the IEF that would result in a correct dry-out power prediction by the codes. The IEF was iterated upon until the film dry-out condition was met at a power within ±3% of the experimental power whilst keeping the same entrainment and deposition correlations. Figure 7 shows the results for the BARC and Harwell cases in a CHF versus mass flux plot to the left, and in a flow regime map to the right. Each experimental case is deemed either:

a) Successful, when a value between zero and unity for the IEF could predict CHF within ±3%
b) Unsuccessful, when no value between zero and unity for the IEF could predict CHF within ±3%. Unsuccessful cases are classed according to whether the iterated IEF has reached unity or zero.

From Figure 7 it can be seen that there is a distinct diagonal line of unsuccessful cases in red. Highlighting the successful cases on the flow regime map shows how the majority fall in the low liquid - high vapour superficial momentum flux region of the plot. There is some overlap with the unsuccessful cases close to the wispy annular flow region but a relatively clean distinction can be made.

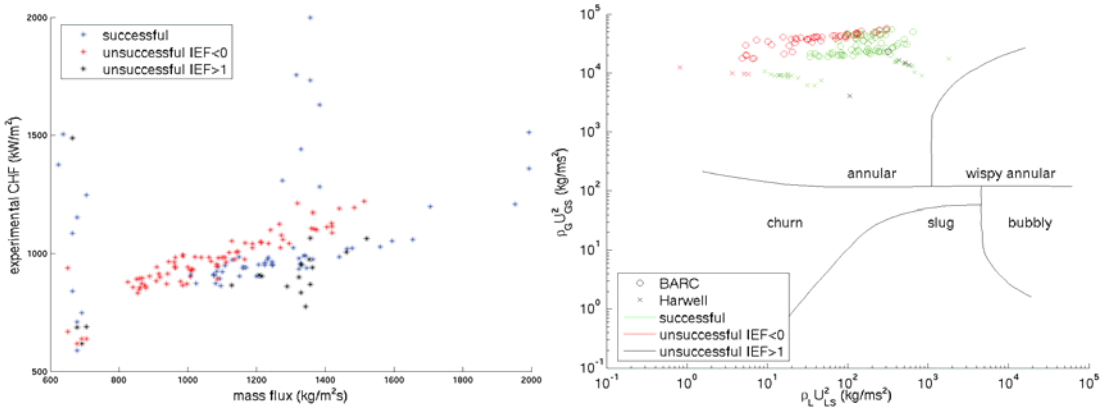

Figure 7. Cases predicted for the physical range of the IEF with Govan [17] correlation

Given the upstream (inlet) boundary condition, the IEF, the rest of the phenomenological model can be simplified as comprising only the evaporation rate, which is fairly reliably computed, and a deposition rate and entrainment rate, both of which are obtained from correlations based on experimental measurements, and thus rather less certain. It thus follows that unsuccessful cases represent conditions in which one or more of the constitutive correlations used in this phenomenological model does not provide an accurate description of the dry-out phenomenon. For these cases, a more accurate (e.g. mechanistic) way of determining the IEF would most likely not cause much improvement in the prediction of the CHF. To investigate this issue further, the IEF iteration was repeated but with the entrainment and deposition correlations from [14]. The results are shown in Figure 8.

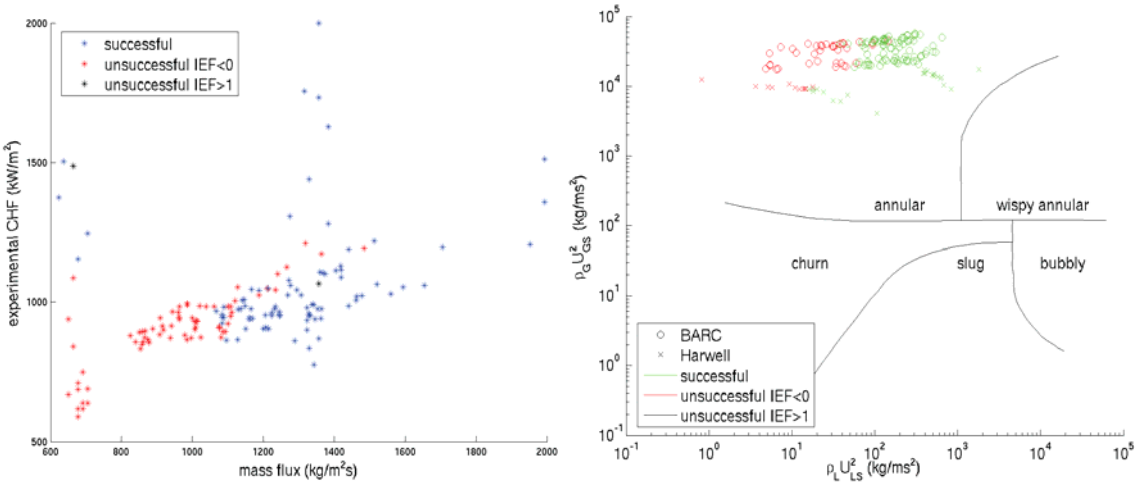

Figure 8. Cases predicted for the physical range of the IEF with Okawa [14] correlation

Figure 8 shows that some of the previous “unsuccessful” cases are now “successful”, especially at the higher mass flux region of the plot while some of the “successful” cases have turned “unsuccessful”. Most of the “unsuccessful” cases occur at the low mass flux, low CHF region of Figure 8. A clearer boundary between the “successful” and “unsuccessful” cases can be seen on the flow regime map for this correlation. Although one can identify these differences in detail, it is striking just what considerable commonality is exhibited between successful and unsuccessful cases despite the change in entrainment and deposition correlations. An in-depth investigation on the causes leading to this observation has not been carried out at this stage.

6. CONCLUSIONS

The reliable knowledge of the margin to critical heat flux plays an important role in nuclear reactor design and operation. Phenomenological modelling is gaining importance in the prediction of film dry-out as use of empirical correlations on their own often fails to predict dry-out for highly varying non-uniform axial heat fluxes. Experimental measurements for all of the multitudinous combinations of conditions and axial power shapes is impractical, and empirically-based extrapolation and interpolation can require costly margins to be provided.

In this paper three independently developed codes (MEFISTO-T, GRAMP and SCADOP) for the mechanistic prediction of film dry-out in annular flow have been validated and cross-verified. Good agreement has been shown against the experimental data for the three codes, with peak errors lower than ± 11%. The correspondence between the codes is also very good with a mean error lower than 2% between the codes.

A sensitivity study has been carried out in order to identify the value of the IEF that can predict the experimental critical heat flux within ± 3%. A range of cases has been identified for which the entrainment and deposition correlations used in the validation is unable to predict CHF for the physical range of the IEF. It has been shown that by changing the entrainment and deposition correlation while keeping the onset of annular flow condition constant, the range of cases that can be successfully predicted changes somewhat, but retains the same general characteristics. It is concluded that phenomenological modelling provides a robust complement to empirical correlations, and that further work on this issue would be valuable.

REFERENCES

1. Y. Katto, "Generalized correlations of critical heat flux for the forced convection boiling in vertical uniformly heated annuli", *International Journal of Heat and Mass Transfer*, **22**(4), pp. 575-584 (1979).
2. D.C. Groeneveld, J.Q. Shan, A.Z. Vasić, L.K.H. Leung, A. Durmayaz, J. Yang, S.C. Cheng, and A. Tanase, "The 2006 CHF look-up table", *Nuclear Engineering and Design*, **237**(15–17), pp. 1909-1922 (2007).
3. M. Ahmad, D.K. Chandraker, G.F. Hewitt, P.K. Vijayan, and S.P. Walker, "Phenomenological modeling of critical heat flux: The GRAMP code and its validation", *Nuclear Engineering and Design*, **254**(0), pp. 280-290 (2013).
4. F. Aydogan, B. Neykov, M. Avramova, L.E. Hochreiter, K. Ivanov, H. Utsuno, E. Sartori, and M. Martin. "Overview and status of the OECD/NRC BFBT benchmark activities", *12th International Topical Meeting on Nuclear Reactor Thermal Hydraulics, NURETH-12, September 30, 2007 - October 4, 2007,* Pittsburgh, PA, United states (2007).
5. C. Adamsson and J.-M. Le Corre, "Modeling and validation of a mechanistic tool (MEFISTO) for the prediction of critical power in BWR fuel assemblies", *Nuclear Engineering and Design*, **241**(8), pp. 2843-2858 (2011).

6. C. Adamsson and J.M. Le Corre, "Transient dryout prediction using a computationally efficient method for sub-channel film-flow analysis", *Nuclear Engineering and Design*, **280**, pp. 316-25 (2014).
7. A. Dasgupta, D.K. Chandraker, P.K. Vijayan, and D. Saha. "A Mechanistic Model Based on Film Depletion for Prediction of Dryout Power in Tubular Geometry", *NURETH-13,* Kanazawa, Japan (2009).
8. A. Dasgupta, D.K. Chandraker, and P.K. Vijayan. "SCADOP: A Computer Code for Steady State Subchannel Analysis of Nuclear Fuel Bundles", *19th National & 8th ISHMT-ASME Heat and Mass Transfer Conference,* JTNU Hyderabad, India (2008).
9. A. Dasgupta, D.K. Chandraker, and P.K. Vijayan. "A Phenomenological Model for Prediction of Dryout in Nuclear Fuel Rod Bundles", *NUTHOS-9,* Kaohsiung, Taiwan (2012).
10. D.K. Chandraker, P.K. Vijayan, R.K. Sinha, and M. Aritomi, "Phenomenological prediction of CHF under boiling water reactor (BWR) conditions", *Progress in Nuclear Energy*, **53**(7), pp. 874-880 (2011).
11. G.F. Hewitt, H.A. Kearsey, P.M.C. Lacey, and D.J. Pulling, "Burnout and nucleation in climbing film flow", *International Journal of Heat and Mass Transfer*, **8**(5), pp. 793-814 (1965).
12. D.K. Chandraker, A.K. Vishnoi, and P.K. Vijayan. "Experimental investigation on critical heat flux and assessment of look-up table approach ", *19th National and 8th ISHMT-ASME HMTC,* Hyderabad, India (2008).
13. G.F. Hewitt and D.N. Roberts, *Studies of Two-Phase Flow Patterns by Simultaneous X-Ray and Flash Photography*, in *Other Information: UNCL. Orig. Receipt Date: 31-DEC-69*. 1969. p. Medium: X; Size: Pages: 28.
14. T. Okawa, A. Kotani, I. Kataoka, and M. Naitoh, "Prediction of the critical heat flux in annular regime in various vertical channels", *Nuclear Engineering and Design*, **229**(2–3), pp. 223-236 (2004).
15. M. Ishii and K. Mishima, "Droplet entrainment correlation in annular two-phase flow", *International Journal of Heat and Mass Transfer*, **32**(10), pp. 1835-1846 (1989).
16. S. Sugawara. "Droplet deposition and entrainment modeling based on the three-fluid model", *Proceedings of the 3rd International Topical Meeting on Nuclear Power Plant Thermal Hydraulics, 14-17 Nov. 1988,* Netherlands 122, pp. 67-84 (1990).
17. G.F. Hewitt and A.H. Govan, "Phenomenological modelling of non-equilibrium flows with phase change", *International Journal of Heat and Mass Transfer*, **33**(2), pp. 229-242 (1990).
18. G.B. Wallis, *One-dimensional two-phase flow*, McGraw-Hill, New York, Maidenhead, (1969).
19. T. Okawa, A. Kotani, I. Kataoka, and M. Naito, "Prediction of critical heat flux in annular flow using a film flow model", *Journal of Nuclear Science and Technology*, **40**(6), pp. 388-396 (2003).
20. J.R. Barbosa, Jr., G.F. Hewitt, G. Konig, and S.M. Richardson, "Liquid entrainment, droplet concentration and pressure gradient at the onset of annular flow in a vertical pipe", *International Journal of Multiphase Flow*, **28**(6), pp. 943-61 (2002).
21. A. Dasgupta, D.K. Chandraker, A.K. Vishnoi, and P.K. Vijayan, "A new methodology for estimation of initial entrainment fraction in annular flow for improved dryout prediction", *Annals of Nuclear Energy*, **75**(0), pp. 323-330 (2015).
22. M. Ahmad, Peng, D.J., Walker, S.P., Hale, C.P., Hewitt G.F.,. "Droplet Entrainment in Churn Flow", *International Conference of Multiphase Flow,* Florida, USA (2010).
23. K. Wang, B. Bai, and W. Ma, "An improved liquid film model to predict the CHF based on the influence of churn flow", *Applied Thermal Engineering*, **64**(1-2), pp. 422-429 (2014).